CHEMISTRY
A EUROPEAN JOURNAL

DOI: 10.1002/chem.200700986

Electronic and Magnetic Properties of Bimetallic Ytterbocene Complexes: The Impact of Bridging Ligand Geometry

Christin N. Carlson, Jacqueline M. Veauthier, Kevin D. John,* and David E. Morris*[a]

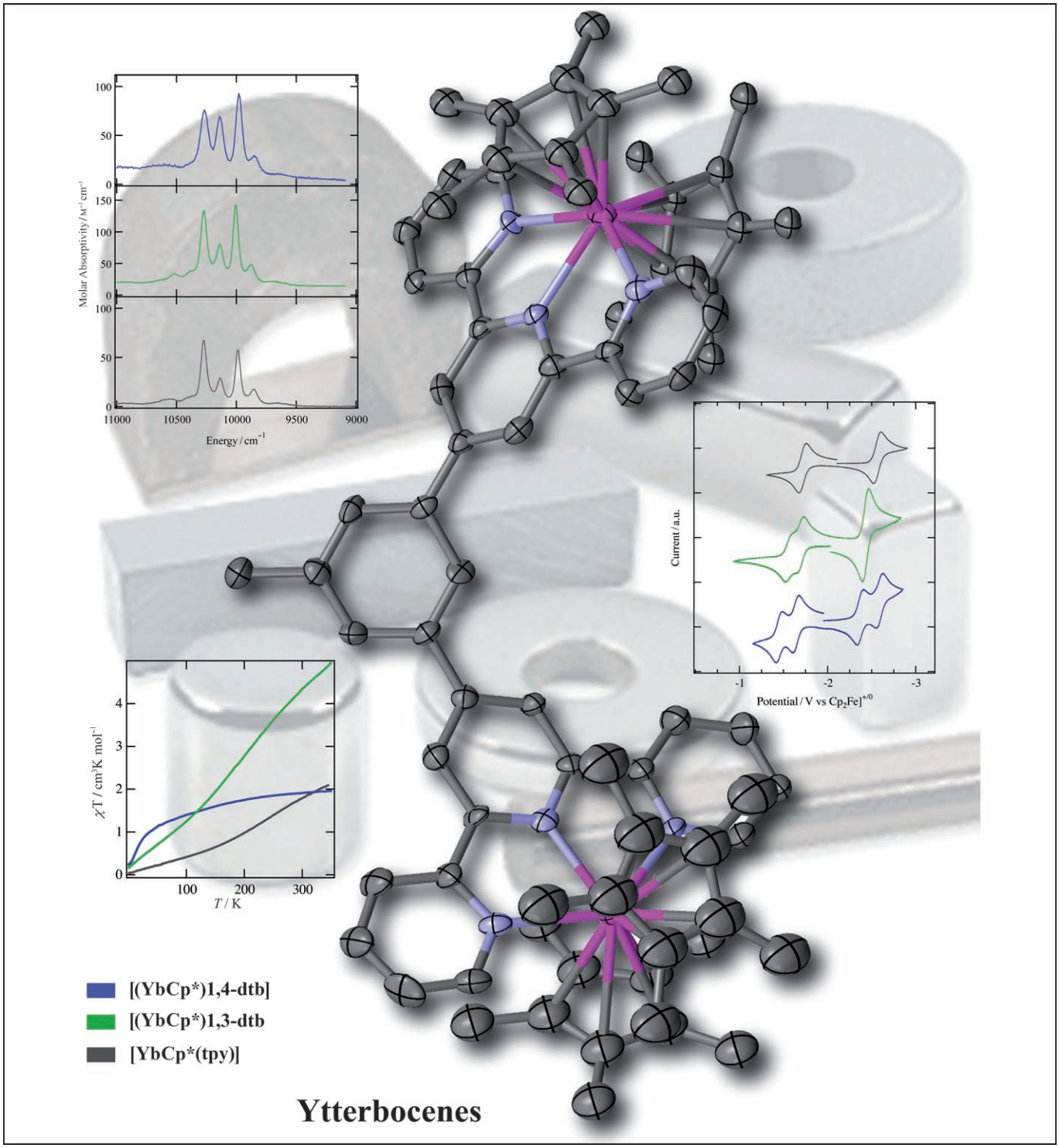

Abstract: Bimetallic ytterbocene complexes with bridging N-heterocylic ligands have been studied extensively in recent years due to their potential applications ranging from molecular wires to single-molecule magnets. Herein, we review our recent results for a series of ytterbocene polypyridyl bimetallic complexes to highlight the versatility and tunability of these systems based on simple changes in bridging ligand geometry. Our work has involved structural, electrochemical, optical, and magnetic measurements with the goal of better understanding the electronic and magnetic communication between the two ytterbium metal centers in this new class of bimetallics.

Keywords: magnetic properties · metallocenes · UV/Vis spectroscopy · ytterbium

Introduction

The concept of designing molecular wires with tunable electronic and magnetic properties has been of great interest to many researchers as a means of bridging the gap between the atomic and bulk scale.[1–14] Discrete assemblies having two metal centers connected by a bridging ligand, which show a pronounced and tunable electronic communication between metal centers, are of particular interest. Ligand-mediated metal–metal interactions allow the possibility of delocalization of electron density over fairly long distances, and in the emerging field of molecular electronics this represents one of the simplest electronic building blocks: a molecular wire. Moreover, the establishment of a controlling mechanism for this communication could potentially lead to switchable logic states, which is essential for the development of the basic elements of molecular electronic and quantum computing devices.[15–17]

Recently, an entirely new class of potential molecular wires has been identified based on the pioneering efforts of Andersen and co-workers on N-heterocyclic-based adducts of ytterbocene.[18–22] The basic building blocks (Scheme 1) in these ytterbocene systems are the neutral bis(cyclopentadienyl) ytterbium bent-metallocene core and a polypyridyl ligand in the metallocene wedge. For a $\{YbCp^*_2\}$ core ($Cp^* = C_5Me_5$) and a very broad range of ligands, a spontaneous charge transfer takes place between the nominally divalent $4f^{14}$ metal and the neutral polypyridyl ligand to give a

[a] Dr. C. N. Carlson, Dr. J. M. Veauthier, Dr. K. D. John, Dr. D. E. Morris
Chemistry Division, Los Alamos National Laboratory
Los Alamos, NM 87545 (USA)
Fax: (+1) 505-667-0440
E-mail: kdjohn@lanl.gov
demorris@lanl.gov

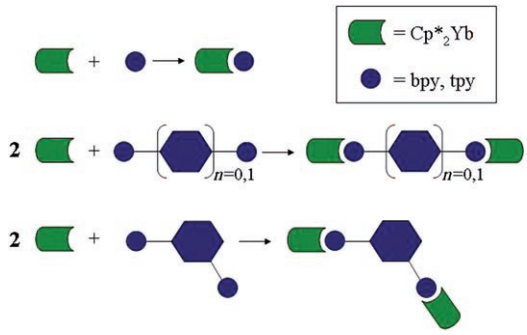

Scheme 1. Building blocks for bimetallic ytterbocene molecular wires.

ground-state electronic configuration of $Yb^{3+}(4f^{13})$–$L^{-}(\pi^{*1})$. This stable charge-transfer ground state has been confirmed by magnetic susceptibility and spectroscopic (NMR, IR, resonance Raman, and electronic) measurements.[18,23] The propensity for this charge-transfer process to occur, the generality and versatility of polypyridyl ligands to function as bridging ligands between metal centers, and the uniqueness of ground-state multimetallic polypyridyl complexes with electrons in antibonding orbitals on the bridging ligand all conspire to make these bimetallic ytterbocene complexes exciting new candidates for molecular wires and other electronic and magnetic applications.

Efforts in our group and others have focused on the systematic characterization of the internal charge-transfer process that exists in monometallic[18,21,23,24] and bimetallic[19,25–28] ytterbocene polypyridyl complexes with the aim of understanding the magnetic/electronic coupling that exists in this class of materials. In the bimetallic systems, the spontaneous charge-transfer process leads to added complexity, since the disposition of two electrons (one from each Yb center) on the bridging ligand can result in many possible electronic configurations. Elaboration and control of these different configurations lies at the heart of our studies, since the disposition of these antibonding electrons is expected to dictate both electronic and magnetic interactions between the metals. Systematic structural variations (i.e., progressively increasing metal–metal distances) have been one of our key areas of focus due in part to the strong analogy between bimetallic ytterbocene complexes and the widely studied transition-metal bimetallic systems such as the Creutz–Taube ion.[29] In particular, the electronic structures of the stable charge-transfer ground states in these ytterbocene complexes (i.e., oxidized metal and reduced ligand) are analogous to the excited electronic states in the d^6 transition-metal polypyridyl complex, $[Ru(bpy)_3]^{2+}$, which have demonstrated potential for a variety of applications in photovoltaic and electrochromic devices.[15,30,31] Furthermore, the ytterbocene charge-transfer complexes are readily manipulated by chemical or electrochemical means, so it may be possible to tune the magnetic interactions between electrons in these multiple-spin systems, providing an added

benefit to ytterbocene-based systems over the classic Ru polypyridyl template. This property is important for applications in the emerging fields of molecular magnetism[32] and spintronics.[33–35]

This review consolidates and integrates recent work in our group on these ytterbocene–polypyridyl systems.[23–28] We have considered not only the effects of increasing the metal–metal separation, but also the effects of changing bridging ligand geometry to alter the symmetry of the metal–metal vectors (Scheme 1). The results for the bimetallic systems are placed in context by comparison to their monometallic analogs and related transition-metal systems. The complexes that are discussed (**1**–**8**) are shown here. Due to the complex nature of these systems, our approach has been to study each complex by cyclic voltammetry, electronic absorption spectroscopy, NMR spectroscopy, single-crystal X-ray crystallography (when crystals form), and magnetic susceptibility. Density functional theory has also been used to aid in understanding the orbital pictures of the various polypyridyl ligands,[27,28] but will not be discussed here.

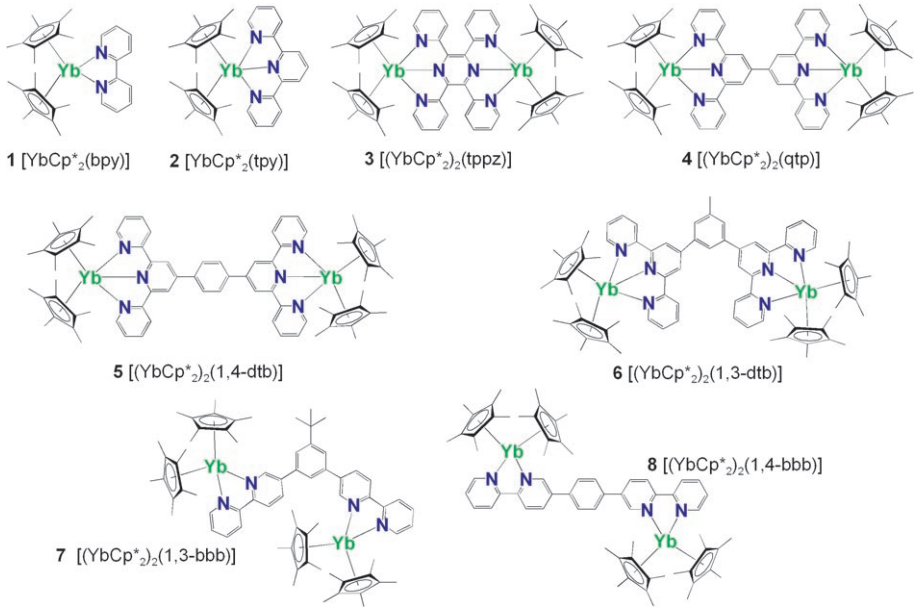

Discussion

Syntheses and structures: The neutral complexes **1**–**8** were prepared by adding a solution of $[YbCp^*_2]\cdot OEt_2$[36] in toluene to the nitrogen ligands at room temperature under inert atmosphere to provide complexes ranging in color from dark green to dark blue in moderate to good yield. The neutral products are soluble in toluene and tetrahydrofuran (THF) and display limited solubility in alkane solvents. In addition, the neutral complexes react with halogenated solvents and there is some evidence that the polypyridyl ligands are displaced by solvent in acetonitrile. The neutral species are quite air and moisture sensitive, decomposing quickly to provide uncharacterized brown material. The intense, deep colors of these materials are a result of the spontaneous charge transfer that occurs upon ligand complexation. The optical spectra (vide infra) are dominated by the π–π* and/or π*–π* transitions associated with the reduced ligands. The oxidation reactions of the neutral complexes were carried out in a straightforward manner employing common oxidants such as ferrocenium hexafluorophosphate, or silver salts (AgX; X = I, SO_3CF_3, PF_6, $B(C_6H_5)_4$, $B(C_6F_5)_4$) in THF resulting in complexes that are typically orange in color. The oxidation products are extracted into methylene chloride and the solvent removed to yield orange to brown powders. The cation complexes display remarkable stability when compared to the neutral species as evidenced by their long-term solution stability and limited air stability.

Despite the large chemical shift window (−48 to 196 ppm) associated with the neutral complexes as a consequence of the charge-transfer induced paramagnetism, ^{1}H NMR spectra were collected for all complexes and are in good agreement with the structures shown above and Figure 1. In some cases, not all proton peaks were identified, presumably due to the presence of the paramagnetic metal centers and/or a radical bridging ligand. Resonances for the dicationic species were more easily defined due to the neutral, diamagnetic status of the bridging ligand. On the basis of these NMR data, the bimetallic complexes were inferred to be highly symmetric in solution suggesting that the polypyridyl moieties freely rotate about the polypyridyl–aryl bond.

X-ray crystal structures were obtained by our group and others for **1**,[18] **2**, **3**, and **6** and cations $\mathbf{1}^+$, $\mathbf{2}^+$,and $\mathbf{3}^{2+}$. A variant of complex **4**, [{Yb-$(C_5EtMe_4)_2$}$_2$(qtp)] (referred to as **4′**), was also obtained. The structures of complexes **2**, **4′**, and **6** are shown in Figure 1. For complex **2**, the tpy ligand is bound in a tridentate manner within the ytterbocene wedge. The central Yb–N bond length is 2.41(1) Å and the outer Yb–N distance is 2.42(1) Å, which is about 0.1 Å longer than reported for **1**.[18] This may be due to a significant steric interaction between the exterior pyridyl groups and the Cp* rings. This interaction is also manifested in the Yb–Cp*(centroid) distances for **2** (2.44 versus 2.32 Å for **1**). However, the Cp*(centroid)-Yb-Cp*(centroid) angle is essentially the same for both complexes (138° for **2** and 139.3° for **1**). Comparison of the bond lengths and bond angles of complex $\mathbf{2}^+$ to **2** reveals that the mean Yb–N bond length (2.44 Å) is slightly elongated relative to the neutral congener **2** (2.41 Å). Furthermore, we observe that the Yb–Cp*-

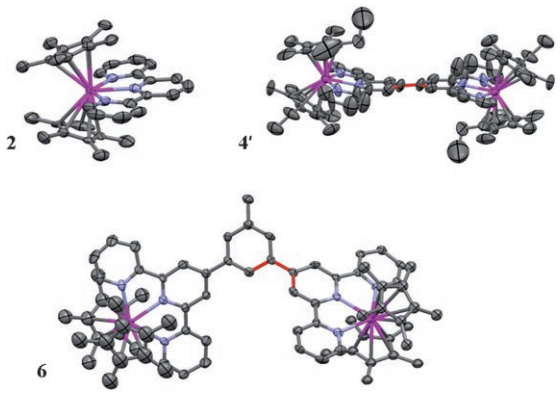

Figure 1. Thermal ellipsoid representation of **2**, **4′**, and **6** (35% probability ellipsoids). The hydrogen atoms have been omitted for clarity. The C_{pyr}-C_{pyr}-C_{Ar}-C_{Ar} torsion angles are shown in red for clarity (**4′** 4.15°; **6** 33.5°). Data from referencees [25–27].

(centroid) bond length of $\mathbf{2}^{+}$ (2.38 Å) contracts relative to **2** (2.44 Å). These trends are consistent with values observed previously for the bpy complex (Table 1) and can be attributed to electrostatic differences between the two redox congeners.[18]

Like $\mathbf{2}^{+}$, a slight elongation of the Yb–N bond lengths and a contraction of the Yb–Cp*(centroid) distance are observed upon oxidation of **3** to $\mathbf{3}^{2+}$ (Table 1). The relatively small changes observed in the aforementioned coordinates for the tppz complexes could be due in part to the fact that the charge can now be distributed between two metal sites. A significant lengthening of the Yb–Yb distance is observed upon oxidation (7.57 Å for **3** and 7.628 Å for $\mathbf{3}^{2+}$),[25] which compares to values between 6.2–6.9 Å reported for transition-metal, η^3-bound, tppz complexes.[5,6,37–45] In addition to the lengthening of the Yb–Yb distance, a relaxation of the ligand torsion angles (C_{pyr}-C_{pyz}-C_{pyz}-C_{pyr} = 55° for **3** and 39° for $\mathbf{3}^{2+}$) is observed and is evidence that steric interactions between the two metal centers are significant.[25] Of the reported bimetallic structures containing the qtp ligand, the average torsion angle between the two tpy portions is approximately 4° and metal–metal separations range from 10.8–11.5 Å.[46–48] For the two reported bimetallic dtb structures, one has a torsion angle (defined by the angle between the bridging aryl group and the tpy portion of the ligand) of 3.6°, while the other possesses an angle of 37.6°; the angle between the two tpy fragments are 6.1 and 2.3°, respectively, with corresponding metal–metal separations of 15.2 and 15.7 Å.[48,49] Our expectation for the qtp (**4′**) and dtb (**6**) geometries discussed here is that the bridging ligands will be nearly planar in the solid state. This is due to the fact that the structure of the related qtp complex **4′** possesses a tpy–tpy torsion angle of 0.4° (see highlighted angle in Figure 1) and a metal separation of 11.8 Å. Furthermore, the electronic behavior of these complexes (vida infra) suggests that there is significant interaction across the bridging ligand, which argues against an orthogonal orientation of the two {YbCp*$_2$(tpy)} fragments.

To the best of our knowledge, the structure for **6** represents the first case of a 2:1 metal-to-ligand adduct of the 1,3-bis(tpy) framework.[50] In fact, it represents only the second structurally characterized case of a 1,3-bis(polypyridyl) complex; the other being a trinuclear copper(I)–bipyridine-based complex.[51] One of the key features of the structure of **6** is that both tpy moieties bind to the ytterbium in a tridentate manner with an average Yb–N distance of 2.391(8) Å and an average Yb–Cp*(centroid) distance of 2.48(1) Å. Both values are statistically indistinguishable from the previously reported monometallic analog **2** with Yb–N(av) and Yb–Cp*(centroid) distances of 2.42(1) and 2.44(1) Å, respectively.[25] Both tpy groups are torsionally rotated out of the plane defined by the tolyl spacer by 26 and 41°. The angle separating the planes defined by the tpy moieties is 56° (see highlighted angle in Figure 1). The Yb–Yb through-space distance is 13.7 Å, which compares to an average value of 15.4 Å for the three transition-metal complexes employing the 1,4-dtb ligand.[48,49,52]

Electrochemistry: Room-temperature voltammetric data for neutral complexes **1**–**8** in 0.1 M $[(n\text{-}C_4H_9)_4N][B(C_6F_5)_4]$/THF are presented in Figure 2. Metrical data extracted from these voltammograms are summarized in Table 2. Although the Yb metal centers in these complexes are generally oxophilic, solutions of the complexes in THF were found to be stable for hours. In fact, while THF is a rather poor solvent for electrochemistry, because of its low dielectic constant, its use is dictated to ensure sample integrity. In more common electrochemical solvents such as acetonitrile, the complexes

Table 1. Selected bond lengths [Å] and angles [°] for **1**, **2**, $\mathbf{2}^{+}$, $\mathbf{3}^{2+}$, **4′**, and **6**.

	1[18]	**2**[25]	$\mathbf{2}^{+}$[26]	**3**[25]	$\mathbf{3}^{2+}$[26]	**4′**[26]	**6**[27]
bond lengths							
Yb–N_{mean}	2.32	2.41	2.44	2.43	2.45	2.404(7)	2.391(8)
Yb–$N_{central}$	NA	2.41(1)	2.440(9)	2.42(1)	2.438(9)	2.327(7)	2.334(7)
Yb–$N_{terminal}$	NA	2.42(1)	2.433(9)	2.43(1)	2.452(9)	2.449(7), 2.436(7)	2.419(8)
Yb–Yb	N/A	N/A	N/A	7.57	7.628	11.809	13.7
Yb–Cp*$_{cent}$	2.34	2.44	2.38	2.42	2.406	2.418	2.48(1)
bond angles (ave)							
Cp*$_{cent}$-Yb-Cp*$_{cent}$	139.3	138.3	N/A	140	139.2	135.62	137.2
C_{pyr}-C_{pyr}-C_{Ar}-C_{Ar}	N/A	N/A	N/A	55	39	N/A	N/A
C_{pyr}-C_{pyr}-$C_{Ar(pyr)}$-$C_{Ar(pyr)}$	N/A	N/A	N/A	N/A	N/A	4.15	33.5
N_{pyr}-C_{pyr}-$C_{pyr(pyz)}$-N_{pyz}	3	1	3	24	18	12.7	4.1

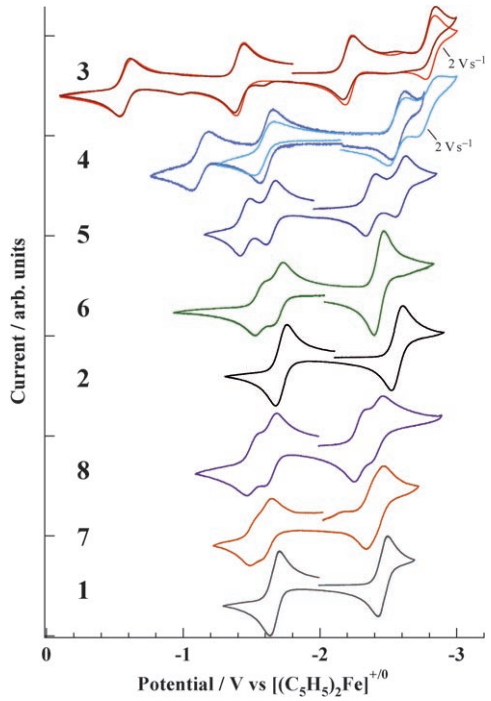

Figure 2. Cyclic voltammograms at a Pt disk working electrode in 0.1 M ([(*n*-$(C_4H_9)_4N$][$B(C_6F_5)_4$]/THF at room temperature of complexes **1**–**8**. Scan rates were 200 mV s^{-1}. unless indicted otherwise. Concentrations of all analytes were ≈5 mM. Currents are in arbitrary units to facilitated comparisons. Data from references [23, 25–28].

readily decompose. Note, however, that when using low dielectric solvents like THF, the choice of electrolyte is crucial to ensure optimal voltammetric behavior. As noted in several recent reports, [(*n*-$C_4H_9)_4N$][$B(C_6F_5)_4$] and similar fluorinated phenyl borate salts provide the necessary solution conductivity to make these studies possible.[53–55]

For the monometallic complexes **1** and **2**, all physical characterization data (magnetic susceptibility, NMR, optical) attest to the dominance of the paramagnetic [$4f^{13}$–π^{*1}] $Yb^{III}L^{\bullet-}$ species at room temperature in the solid state and in solution. Thus, the voltammetric waves must be ascribed to a metal-based one-electron reduction step ($4f^{13}\rightarrow 4f^{14}$) and a ligand-based one-electron oxidation step ($L^{\bullet-}\rightarrow L^0$).[23] For the bimetallic complexes, **3**–**5**, **7**, and **8**, there are two reduction waves and two oxidation waves observed in the potential region from ≈0 to −3.0 V versus $[(C_5H_5)_2Fe]^{+/0}$ (Figure 2). These four waves are all chemically reversible one-electron processes at all scan rates with the exception of the second reduction wave for **3** and **4** that becomes reversible only at fast scan rates.

Assignments for these voltammetric waves for the bimetallic systems follow from the results described above for the monometallic complexes. Specifically, the two reduction waves are attributed to a one-electron reduction of each metal center, and the oxidation waves are attributed to two successive one-electron oxidation steps for the doubly-reduced bridging ligand. Complex **6** also exhibits two reversible, bridging ligand-based oxidation waves; however, the most notable feature in the voltammetric properties of **6** relative to all other bimetallic ytterbocene complexes we have investigated is that only a single metal-based reduction wave is observed in this potential region.[27]

The most salient voltammetric parameter to assess electronic interactions between metal centers in these bimetallic systems is the potential separation between the waves associated with the metal-based processes ($\Delta(E_{1/2})[M_A–M_B]$ in Table 2). In the absence of any metal–metal interaction, one might expect the metal-based processes to occur at the same potential (i.e., two superimposed one-electron waves) with perhaps a slight offset (≈36 mV) due to statistical (entropic) factors.[56] The actual value is quite large for **3** (600 mV), for which the metal–metal distance is smallest (7.57 Å), but remains significant even for the bridging-ligand complexes with larger metal–metal separation (220 mV for both **4** and **5**). Notably, for the corresponding bimetallic ruthenium complexes (for which the pertinent metal-based voltammetric waves are oxidative in nature), the separation is ≈300 mV for the tppz system, but goes to zero for both qtp and dtb. The value for **8** (230 mV) is com-

Table 2. Summary and comparison of redox data[a] for ytterbocene complexes and ruthenium(II) congeners.[b]

	Ligand-based		Metal-based				
	$E_{1/2}$ (L_1)	$E_{1/2}$ (L_2)	$E_{1/2}$ (M_A)	$E_{1/2}$ (M_B)	$\lvert\Delta E_{1/2}\rvert$ [M–L][c]	$\lvert\Delta E_{1/2}\rvert$ [M_A–M_B]	$\lvert\Delta E_{1/2}\rvert$ [L_a–L_b]
1	−1.67	N/A	−2.46	N/A	0.79	N/A	N/A
2	−1.72	N/A	−2.56	N/A	0.84	N/A	N/A
3	−0.58	−1.41	−2.21	−2.81	0.80	0.60	0.83
4	−1.12	−1.61	−2.57	−2.79	0.96	0.22	0.49
5	−1.45	−1.64	−2.37	−2.59	0.73	0.22	0.19
6	−1.56	−1.70	−2.43	N/A	0.73	0	0.14
7	−1.50	−1.63	−2.36	−2.45	0.73	0.09	0.13
8	−1.50	−1.66	−2.20	−2.43	0.54	0.23	0.16
$[(Ru)_2(tppz)]^{4+}$	−0.35	−0.85	1.40	1.70	1.75	0.30	0.50
$[(Ru)_2(qtp)]^{4+}$	−0.93	−1.24	1.31[d]	N/A	2.24	0	0.31
$[(Ru)_2(1,4\text{-dtb})]^{4+}$	−1.18[d]	N/A	1.27[d]	N/A	2.35	0	0

[a] All values in volts. $E_{1/2}$ values are versus $[(C_5H_5)_2Fe]^{+/0}$ in 0.1 M [(*n*-$C_4H_9)_4N$][$B(C_6F_5)_4$]/THF at room temperature. [b] The $(Ru)_2$ unit refers to $\{(ttpy)Ru\}_2$ in which ttpy = 4′-tolyl-2,2′:6′,2″″-terpyridine. Data for $[(Ru)_2(BL)]^{4+}$ (BL = tppz, qtp, 1,4-dtb) in 0.1 M [(*n*-$C_4H_9)_4N$]BF_4/CH_3CN versus SCE at room temperature from reference [57]. [c] Separation in $E_{1/2}$ values between the closest metal- and ligand-based voltammetric waves. This parameter is a rough measure of the stability of the spontaneously formed charge-transfer state in the ytterbocene systems. [d] Assigned as a two-electron process, reference [57].

parable to that observed for the 1,4-substituted tpy-based dimer (**5**; 220 mV), indicating some weak interaction between the metal centers in **8**, while the value for **7** (90 mV) is approaching the limit of noninteracting metal centers. Finally, for **6** the reduction processes for the two metals have collapsed into a single wave indicating that the metal–metal interaction is negligible. A more detailed analysis of the peak current behavior of the reduction wave for **6** versus scan rate shows that it is not a concerted $2e^-$ process, but is instead a simple overlap in potential of two $1e^-$ steps.[27]

We have also included in Table 2 the published data for the structurally related bimetallic ruthenium complexes of these same bridging ligands[2,57] to provide a valuable baseline for comparison of metal–metal interactions across nearly identical bridging-ligand distances. A key difference between the ytterbocene systems and the corresponding bimetallic ruthenium complexes is the electronic configuration on the bridging ligand. For the ytterbocene complexes, the metal-based reduction waves occur in the presence of a doubly reduced bridging ligand. For the ruthenium complexes, the metal-based oxidation waves occur with a neutral ligand connecting the metal centers. Apparently, electron occupation in the antibonding ligand orbital greatly facilitates the redox communication between metals in the ytterbocene complexes.

As a final note on the voltammetric data, we have attempted throughout the course of these investigations to understand and compare the ligand-based redox processes as they, too, should provide information on the disposition of the electrons on the bridging ligand in the neutral (doubly-reduced ligand) bimetallic complexes. All uncomplexed bridging ligands exhibit two or more one-electron reduction waves.[25–28] For simple polypyridyl ligands, the first two reduction waves are typically attributed to the sequential addition of two electrons into the lowest unoccupied π^* molecular orbital to give the radical anion and dianion, respectively.[58] In these cases, the spacing between the waves can be associated loosely with the electron spin-pairing energy in the same orbital. The observed behavior in our systems is not so simple, presumably because most bridging ligand, in their unligated state in particular, are able to adopt twisted geometries that would tend to spatially localize the low-lying π^* orbitals on separate ends of the bridge. Further, we see no strong correlation between the separation of the reduction waves for the unligated systems and the separation of the oxidation waves in the bimetallic complexes (which correspond in principle to removal of the same electrons as added in the free ligand reduction steps). The absence of a correlation is believed to provide evidence for different bridging ligand geometries for the free ligand and the coordinated ligand, because of structural restrictions imposed by the presence of the $\{YbCp^*_2\}$ metal fragments.

Optical spectroscopy: UV/Vis/near-IR electronic absorption spectral data have been obtained for complexes **1**–**8** as neutral species in THF, and $\mathbf{1}^+$, $\mathbf{2}^+$,and $\mathbf{3}^{2+}$–$\mathbf{8}^{2+}$ as cationic species in either CH_2Cl_2 or THF. The complexity of these spectral data precludes a detailed assignment of all observed electronic transitions. Instead, our focus has been on the spectral commonalities and differences between and among the complexes in the different oxidation states, concentrating on aspects that will assist in assigning the ground-state electronic configurations and might reflect the degree to which the metal centers in the bimetallic complexes interact.

Neutral complexes: The optical spectral data for the neutral complexes (Figure 3) show good correspondence with respect to the number, energy, and intensity of the bands among the complexes in the bpy-based series (**1**, **7**, **8**). However, there is greater variability in these data among the complexes in the tpy-based series (**2**–**6**) that reflects changes in the electronic configurations for these species with changing geometries as described in more detail below. All complexes possess a series (three to four) of vibronically struc-

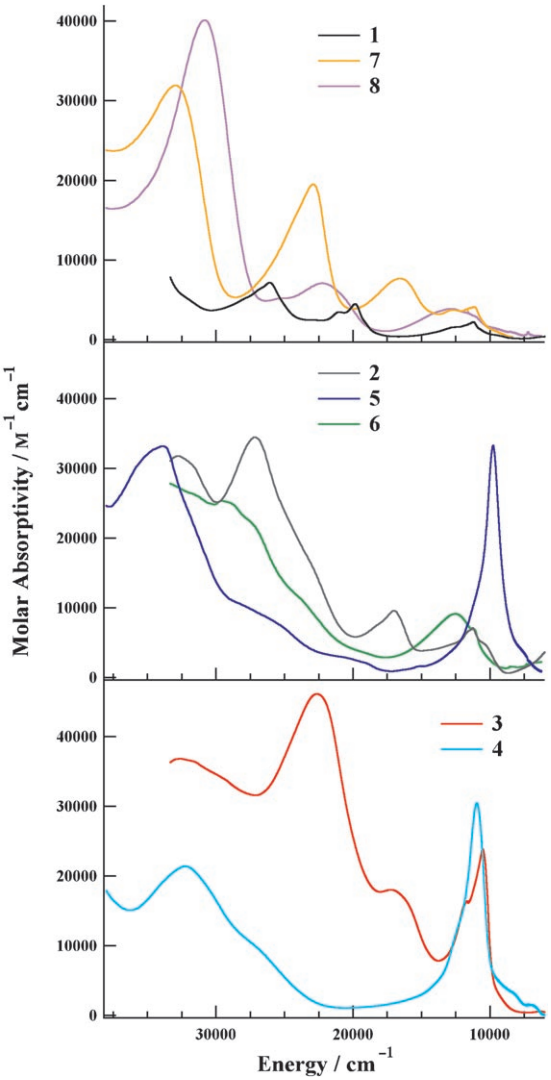

Figure 3. Electronic absorption spectra for neutral species **1**–**8** in THF. Data from references [23,25–28].

tured bands of moderate to high intensity that spans the near ultraviolet and visible regions of the spectra. The intensities suggest that these electronic transitions are electric dipole allowed, and the bandwidths and varying degrees of vibronic structure indicate that there are Frank-Condon active vibrational modes coupled to these electronic states. The occurrence of these intense bands well into the visible spectral region is a clear indicator that the bridging ligands are in all cases in a reduced state with electrons in π^* orbitals. The UV/Vis region for complex **3** has these transitions shifted to even lower energy than seen for the other complexes and reflects the unusual electronic properties of complexes of the tppz ligand.

Substantial differences can be found in spectral comparisons of bimetallic complexes **3–5** versus complexes **6–8**. Two significant observations capture these differences and enable us to make definitive assignments of the ground-state electronic configuration for these bimetallic complexes. First, in monometallic systems **1** and **2**, the principal bands at $\approx 17000\ cm^{-1}$ and $\approx 11000\ cm^{-1}$ have been attributed to polypyridyl-ligand-based transitions derived from the open-shell radical-anion configuration on the basis of observations of nearly identical bands in alkali-metal-reduced free bpy[23] and tpy.[26] These bands are, in effect, signatures for the radical electronic structure of an open-shell ligand . Second, for complexes **3–5**, the NIR spectral region is dominated by the very intense, narrow band at $\approx 10000\ cm^{-1}$ that has been assigned to a transition derived from the doubly reduced ligand dianion. This dominant feature is the hallmark of the singlet dianion bridging ligand structure (i.e., $(\pi^*)^2$).[26] Note that the band energies and widths in the visible region for **6–8** are much more comparable to those for the monometallic complexes **1** and **2** than are those in the bimetallic complexes in **3–5**. Further, there is no evidence for the diagnostic $\approx 10000\ cm^{-1}$ band in the spectrum of complexes **6–8**. Thus, the strong correlation in the spectra of monometallic systems **1** and **2** with those of their corresponding bimetallic systems **6–8**, and the absence of the diagnostic transition associated with the singlet dianion bridging ligand in the spectrum of **6–8** lead to a description of the electronic structure in bimetallic species **6–8** as two effectively independent $\{Yb^{3+}Cp^*_2(L^{\bullet-})\}$ moieties with a net electronic configuration of $(4f_A)^{13}(\pi_a^*)^1(\pi_b^*)^1(4f_B)^{13}$. In contrast, the presence of the spectral signature for the bridging ligand dianion leads directly to the assignment of the electronic configuration in **3–5** of $(4f_A)^{13}(\pi^*)^2(4f_B)^{13}$. Thus, the ligand-based orbital housing the two electrons in neutral complexes **3–5** most likely spans the entire ligand framework, whereas in the diradical systems **6–8** there must be a localization of ligand orbitals on each half of the bridging framework with each orbital accommodating one electron.

The presence of $4f^{13}$ metal centers in these neutral species might be expected to engender metal-localized f–f transitions in these spectral data that should be most informative with respect to metal–metal interactions. Unfortunately, these transitions are known to be fairly weak and lie at $\approx 10000\ cm^{-1}$ (vide infra), and therefore are obscured by the much more intense π–π^* and π^*–π^* transition in this region for all the neutral complexes considered here.

Cationic complexes: The optical data for the dicationic species $\mathbf{3}^{2+}$–$\mathbf{8}^{2+}$ and the monometallic cations $\mathbf{1}^+$ and $\mathbf{2}^+$ were collected over the entire UV/Vis/near-IR range. These spectral data are significantly simplified relative to the neutral complex data, because these species no longer possess electrons in polypyridyl-based π^* orbitals that produce the intense transitions throughout the visible and near-IR range. In fact, the absence of ligand-based π^* electrons in these systems provides the means to focus directly on the spectral manifestations of metal–metal interactions, since the potential influence of singlet or triplet ligand diradicals versus singlet dianions on metal communication has been eliminated, leaving only the influences of metal–metal separation and ligand-based structural distortions to consider. The UV/Vis spectral region for all these complexes is comparable and has been discussed in detail elsewhere.[23,25–28] Here, we focus on the important new spectral feature, namely the emergence of the f–f transitions deriving from the $4f^{13}$ electronic configuration for the ytterbium center(s).

Figure 4 shows the striking energy and intensity comparison of the f–f spectral region for the (di)cationic complexes. Of the tpy-based systems, the behavior of $\mathbf{3}^{2+}$ is clearly the outlier because both principal peak positions and intensities differ from those observed for the other tpy-based (di)cations. These spectral data for $\mathbf{3}^{2+}$ clearly illustrate a much stronger electronic perturbation reflecting significant metal–metal interaction across this shortest of metal–metal distances. For the other tpy-based systems ($\mathbf{2}^+$, $\mathbf{4}^{2+}$, $\mathbf{5}^{2+}$,and $\mathbf{6}^{2+}$), the energies of the principal peaks are nearly identical, and one must turn to intensity considerations to discern differences. Specifically, the integrated intensities in the bands for $\mathbf{4}^{2+}$ and $\mathbf{5}^{2+}$ are $\approx 2\times$ that of $\mathbf{2}^+$. However, careful consideration of the individual lineshapes in the spectrum of $\mathbf{4}^{2+}$ suggests that each principal band is in fact two very closely spaced, narrower bands similar to those seen in $\mathbf{2}^+$, but unresolvable at this level of spectral resolution. A similar situation exists for the bands in $\mathbf{5}^{2+}$, but here the spacing between unresolved features is even smaller than in the spectrum of $\mathbf{4}^{2+}$. This interpretation is consistent with a very small metal–metal interaction in $\mathbf{4}^{2+}$ that leads to a small, but noticeable splitting of the f–f transitions, and an essentially negligible metal–metal interaction over the larger bridging ligand separation in $\mathbf{5}^{2+}$, such that the integrated intensities approximately double without individual band splittings. Finally, the data for $\mathbf{6}^{2+}$ are consistent with the electrochemical result indicating that the metal–metal interaction has been turned off. For this system the band positions and relative intensities are identical to those found in the monometallic cation ($\mathbf{2}^+$), but here the peak intensities (as well as the integrated intensities) increase by $2\times$ relative to those in $\mathbf{2}^+$.

The f–f spectral region of the bpy-based systems ($\mathbf{1}^+$, $\mathbf{7}^{2+}$, and $\mathbf{8}^{2+}$; Figure 4 right panel) portrays a situation similar to that found for the tpy-based systems. Here the peak ener-

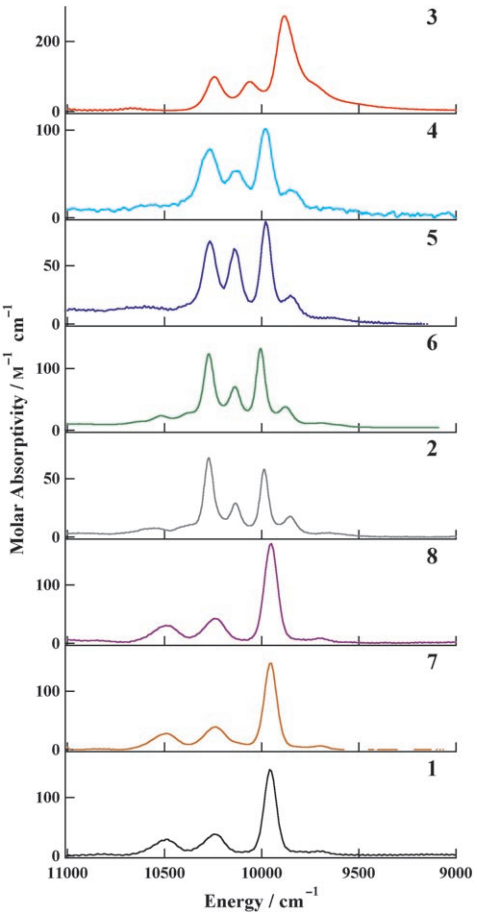

Figure 4. The f–f NIR region for dicationic bimetallic and cationic monometallic complexes in CH_2Cl_2 or THF. Data from references [23,25–28].

gies and relative intensities for the bimetallic dications are identical to those found for the monometallic cation. However, the absolute intensity comparison among these spectra provides no additional insights. Surprisingly, the intensities in the individual bands remain unchanged across this series of complexes. Thus, while the comparability in band energies and relative intensities reflects a lack of metal–metal interaction as expected based on the electrochemical result, the invariance in intensity (particularly in comparison to the behavior seen in $\mathbf{6}^{2+}$ vs. $\mathbf{2}^{+}$) between monometallic and bimetallic systems remains puzzling. We know of no published reports making the direct comparison of f–f spectral data for structurally homologous single-molecule monometallic versus bimetallic lanthanide or actinide complexes.

Magnetic susceptibility: Susceptiblity data were obtained on microcrystalline samples sealed in borosilicate glass NMR tubes as described in detail previously.[24,26–28] The monometallic complexes **1** and **2** are interesting in that they do not obey the Curie–Weiss law, and they have room-temperature magnetic moments of 2.4 and 3.77 μ_B respectively, which are lower than expected for a simple Yb^{III} ion and an uncoupled organic radical (4.85 μ_B).[18] The differences in the observed magnetic moments of these complexes from that predicted for uncoupled moments have been attributed, in the case of **1**, to antiferromagnetic coupling of the Yb^{III} and organic radical unpaired electrons.[18] The complexity of the Yb^{III}-ion/ligand-radical coupling remains a source of intense analysis that is presently being addressed with additional techniques such as magnetic circular dichrosim (MCD) to more completely describe the nature of the magnetic coupling interaction.

The magnetic susceptibilities (χ) for compounds **2**–**8** were measured as a function of temperature (Figure 5). The dependence observed for the χ^{-1} versus T plots reveals that complexes **3** and **5** obey the Curie–Weiss law to approximately 50 K. Below 50 K the χ^{-1} versus T data begin to diverge from linearity. For **4**, the χ versus T data increase and achieve a maximum at approximately 13 K. This feature is reproducible for multiple samples prepared from different formulations and is indicative of Yb^{III}–Yb^{III} antiferromagnetic spin exchange of the type Yb(α)BL(αβ)Yb(β) (BL = bridging ligand) in which the dianionic bridging ligand serves to mediate the metal–metal interaction. For complex **5**, a weak feature at around 10 K is observed that has been ascribed to an antiferromagnetic coupling effect. The basis of the observed low temperature magnetic coupling behav-

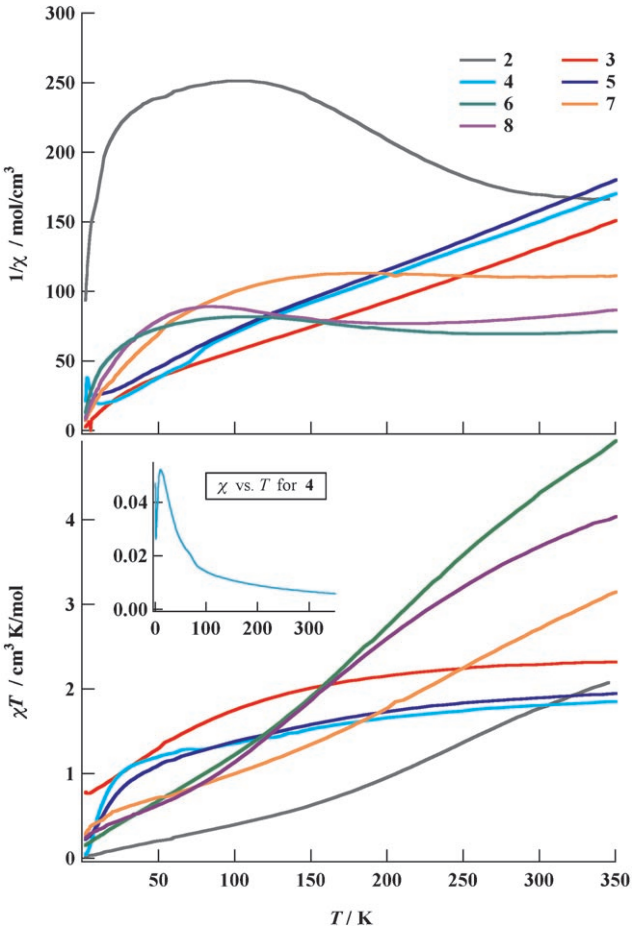

Figure 5. $1/\chi$ (top) and χT (bottom) versus T for complexes **2**–**8** as microcrystalline solids at 0.1 T. Data from references [25–28].

ior arises due to the observed electronic ground state $[(4f)^{13}\text{-}(\pi^*)^2\text{-}(4f)^{13}]$ associated with **5**.

The χ^{-1} versus T plots for complexes **6–8** depart dramatically from the Curie law and exhibit a temperature-dependent profile reminiscent of monometallic analogs such as complexes **1**, **2**, and $[YbCp^*_2(4'\text{-CN-tpy})]$.[24] This monometallic-like behavior would suggest that the 1,3-geometry in **6** and **7** has inhibited magnetic coupling across the bridging ligand. Surprisingly, the 1,4-geometry in **8** has also caused this inhibition unlike the behavior observed in the linear tpy complexes **3–5**. Furthermore, the behavior observed in **6–8** is consistent with the two ytterbocene/tpy or the two ytterbocene/bpy moieties behaving as independent magnetic units. Thus, the spin interactions between each Yb^{3+} ion and its localized ligand radical must dominate the interaction between the two spatially isolated ligand radicals on the bridge. This would result from a poor spin delocalization onto the phenyl bridge fragment due to inherently poor electronic communication across the 1,3/1,4-(2,2′-bipyridyl)-C_6H_4 unit and/or substantial ring torsions about the bpy−Ph bonds. Elucidating the sign and magnitude of the exchange coupling between the metal and ligand-radical spin carriers in this limit is complicated due to the presence of trace magnetic impurities leading to Curie tails and potential subtle differences in ligand field effects. Based on recent unpublished results for complexes **1** and **2** from MCD analysis, we are hopeful that similar studies on the bimetallic systems will shed light on the magnetic behavior of these unique complexes.

Conclusion

The X-ray, NMR spectroscopic, electrochemical, optical, and magnetic characterization described herein for bimetallic ytterbocene complexes clearly illustrate the effects of the bridging polypyridyl ligand geometry on the electronic and magnetic behavior associated with these complexes. At the most fundamental level, the bridging ligand geometries and coordination modes have been found to dictate the electronic configuration on the ligand that derives from the spontaneous charge transfer from the two metal centers. The linear tpy-based bimetallic systems (**3–5**) all exhibit a singlet dianion structure $[(4f_A)^{13}\text{-}(\pi^*)^2\text{-}(4f_B)^{13}]$, even though **4** and **5** could in principle undergo a torsional distortion within the bridge that might break symmetry and localize the ligand spins. All other bimetallic complexes, even **8** which possesses a linear bridging ligand motif, are best described as having a diradical bridging ligand $[(4f_A)^{13}\text{-}(\pi^*_a)^1\text{-}(\pi^*_b)^1\text{-}(4f_B)^{13}]$. These diradical complexes appear to have spatially isolated radicals such that the $YbCp^*_2$–polypyridyl moieties behave in the same manner as their respective monometallic analogues. This localization of spins on the bridging ligand may be a consequence of a dominant metal–radical interaction and/or a torsional distortion within the bridging ligand that breaks symmetry, but our data are inconclusive on this point. It is clear that the metal–radical interaction (as opposed to metal–metal or radical–radical) dominates the magnetic and electronic coupling in these diradical systems, since both bulk susceptibility and electronic spectroscopic behavior mirror that found in the monometallic analogues. In contrast to these diradical complexes, the singlet dianionic systems show enhanced metal–metal coupling in both magnetic and electronic domains, and the anticipated dependence of the strength of electronic coupling on the intermetallic separation is clearly observed. Ongoing studies are implementing magnetic circular dichroism spectroscopy to isolate the f–f transitions in the neutral complexes to better understand the magnetic coupling interactions in these complexes. In addition, new ligand architectures to create trimetallic systems in which spin frustration may be present are being pursued.

Acknowledgements

Funding for this work was provided by Los Alamos National Laboratory's Laboratory Directed Research and Development program and by the U.S. Department of Energy, Office of Basic Energy Sciences under the auspices of the Heavy Element Chemistry program. This work was carried out under the auspices of the National Nuclear Security Administration of the U.S. Department of Energy at Los Alamos National Laboratory under Contract No. DE-AC52–06 A25396. C.N.C. thanks the Seaborg Institute for a postdoctoral fellowship. We also thank Drs. C. J. Kuehl, J. D. Thompson, and B. L. Scott for synthetic and experimental input and Prof. M. L. Kirk for helpful discussions.

[1] M. M. Richter, K. J. Brewer, *Inorg. Chem.* **1992**, *31*, 1594–1598.
[2] C. R. Arana, H. D. Abruna, *Inorg. Chem.* **1993**, *32* 194–203.
[3] F. Barigelletti, L. Flamigni, V. Balzani, J. P. Collin, J. P. Sauvage, A. Sour, E. C. Constable, A. M. W. C. Thompson, *Coord. Chem. Rev.* **1994**, *132*, 209–214.
[4] L. M. Vogler, S. W. Jones, G. E. Jensen, R. G. Brewer, K. J. Brewer, *Inorg. Chim. Acta* **1996**, *250*, 155–162.
[5] M. Graf, H. Stoeckli-Evans, A. Escuer, R. Vicente, *Inorg. Chim. Acta* **1997**, *257*, 89–97.
[6] C. M. Hartshorn, N. Daire, V. Tondreau, B. Loeb, T. J. Meyer, P. S. White, *Inorg. Chem.* **1999**, *38*, 3200–3206.
[7] A. K. Bilakhiya, B. Tyagi, P. Paul, *Polyhedron* **2000**, *19*, 1233–1243.
[8] M. D. Ward, F. Barigelletti, *Coord. Chem. Rev.* **2001**, *216*, 127–154.
[9] S. E. Page, A. Flood, K. C. Gordon, *J. Chem. Soc. Dalton Trans.* **2002**, 1180–1187.
[10] C. Metcalfe, S. Spey, H. Adams, J. A. Thomas, *J. Chem. Soc. Dalton Trans.* **2002**, 4732–4739.
[11] C. Di Pietro, S. Serroni, S. Campagna, M. T. Gandolfi, R. Ballardini, S. Fanni, W. R. Browne, J. G. Vos, *Inorg. Chem.* **2002**, *41*, 2871–2878.
[12] R. S. Bitzer, R. P. Pereira, A. M. Rocco, J. G. S. Lopes, P. S. Santos, M. A. C. Nascimento, C. A. L. Filgueiras, *J. Organomet. Chem.* **2006**, *691*, 2005–2013.
[13] S. Flores-Torres, G. R. Hutchison, L. J. Soltzberg, H. D. Abruna, *J. Am. Chem. Soc.* **2006**, *128*, 1513–1522.
[14] T. E. Janini, J. L. Fattore, D. L. Mohler, *J. Organomet. Chem.* **1999**, *578*, 260–263.
[15] M. D. Ward, *Chem. Soc. Rev.* **1995**, *24*, 121–134.
[16] D. Astruc, *Acc. Chem. Res.* **1997**, *30*, 383–391.
[17] N. Robertson, C. A. McGowan, *Chem. Soc. Rev.* **2003**, *32*, 96–103.
[18] M. Schultz, J. M. Boncella, D. J. Berg, T. D. Tilley, R. A. Andersen, *Organometallics* **2002**, *21*, 460–472.
[19] D. J. Berg, J. M. Boncella, R. A. Andersen, *Organometallics* **2002**, *21*, 4622–4631.

[20] M. D. Walter, M. Schultz, R. A. Andersen, *New J. Chem.* **2006**, *30*, 238–246.
[21] M. D. Walter, D. J. Berg, R. A. Andersen, *Organometallics* **2007**, *26*, 2296–2307.
[22] M. D. Walter, D. J. Berg, R. A. Andersen, *Organometallics* **2006**, *25*, 3228–3237.
[23] R. E. Da Re, C. J. Kuehl, M. G. Brown, R. C. Rocha, E. D. Bauer, K. D. John, D. E. Morris, A. P. Shreve, J. L. Sarrao, *Inorg. Chem.* **2003**, *42*, 5551–5559.
[24] J. M. Veauthier, E. J. Schelter, C. J. Kuehl, A. E. Clark, B. L. Scott, D. E. Morris, R. L. Martin, J. D. Thompson, J. L. Kiplinger, K. D. John, *Inorg. Chem.* **2005**, *44*, 5911–5920.
[25] C. J. Kuehl, R. E. Da Re, B. L. Scott, D. E. Morris, K. D. John, *Chem. Commun.* **2003**, 2336–2337.
[26] C. N. Carlson, C. J. Kuehl, R. E. Da Re, J. M. Veauthier, E. J. Schelter, A. E. Milligan, B. L. Scott, E. D. Bauer, J. D. Thompson, D. E. Morris, K. D. John, *J. Am. Chem. Soc.* **2006**, *128*, 7230–7241.
[27] C. N. Carlson, B. L. Scott, R. L. Martin, J. D. Thompson, D. E. Morris, K. D. John, *Inorg. Chem.* **2007**, *46*, 5013–5022.
[28] C. N. Carlson, C. J. Kuehl, L. Ogallo, D. A. Shultz, J. D. Thompson, M. L. Kirk, R. L. Martin, K. D. John, D. E. Morris, *Organometallics* **2007**, *26*, 4234–4242.
[29] W. Kaim, A. Klein, M. Glockle, *Acc. Chem. Res.* **2000**, *33*, 755–763.
[30] *"Photoinduced Electron Transfer in Metal–Organic Dyads"*: K. S. Schanze, K. A. Walters, in *Molecular and Supramolecular Photochemistry* (Eds.: V. Ramamurthy, K. S. Schanze), Marcel Dekker, **1998**.
[31] V. Balzani, A. Juris, M. Venturi, S. Campanga, S. Serroni, *Chem. Rev.* **1996**, *96*, 759–833.
[32] E. Coronado, F. Palacio, J. Veciana, *Angew. Chem.* **2003**, *115*, 2674–2676; *Angew. Chem. Int. Ed.* **2003**, *42*, 2570–2572; .
[33] A. R. Rocha, V. M. Garcia-Suarez, S. W. Bailey, C. J. Lambert, J. Ferrer, S. Sanvito, *Nat. Mater.* **2005**, *4*, 335–339.
[34] S. Sanvito, A. R. Rocha, *J. Comput. Theor. Nanosci.* **2006**, *3*, 624–642.
[35] A. J. Epstein, *MRS Bull.* **2003**, *28*, 492–499.
[36] T. D. Tilley, J. M. Boncella, D. J. Berg, C. J. Burns, R. A. Andersen, *Inorg. Synth.* **1990**, *27*, 146.
[37] C. S. Campos-Fernández, B. W. Smucker, R. Clérac, K. R. Dunbar, *Isr. J. Chem.* **2001**, *41*, 207–218.
[38] J. Carranza, C. Brennan, J. Sletten, J. M. Clemente-Juan, F. Lloret, M. Julve, *Inorg. Chem.* **2003**, *42*, 8716–8727.
[39] N. Chanda, R. H. Laye, S. Chakraborty, R. L. Paul, J. C. Jeffery, M. D. Ward, G. K. Lahiri, *J. Chem. Soc. Dalton Trans.* **2002**, 3496–3504.
[40] M. Graf, B. Greaves, H. Stoeckli-Evans, *Inorg. Chim. Acta* **1993**, *204*, 239–246.
[41] D. Hagrman, P. Hagrman, J. Zubieta, *Inorg. Chim. Acta*, **2000**, *300–302*, 212–224.
[42] M. Koman, Z. Balaghova, D. Valigura, *Acta. Crystallogr. Sect. C* **1998**, *54*, 1277.
[43] K. Sakai, M. Kurashima, *Acta Crystallogr. Sect. E* **2003**, *59*, m411–413.
[44] W. Teles, N. L. Speziali, C. A. L. Filgueras, *Polyhedron* **2000**, *19*, 739–742.
[45] Y. Yamada, Y. Miyashita, K. Fujisawa, K. Okamoto, *Bull. Chem. Soc. Jpn.* **2000**, *73*, 1843–1844.
[46] W. Ouellette, V. Golub, C. J. O'Connor, J. Zubieta, *Dalton Trans.* **2005**, 291–309.
[47] B.-K. Koo, W. Ouellette, E. M. Burkholder, V. Golub, C. J. O'Connor, J. Zubieta, *Solid State Sci.* **2004**, *6*, 461–468.
[48] B.-K. Koo, L. Bewley, V. Golub, R. S. Rarig, E. Burkholder, C. J. O'Connor, J. Zubieta, *Inorg. Chim. Acta* **2003**, *351*, 167–176.
[49] M. Maekawa, T. Minematsu, H. Konaka, K. Sugimoto, T. Kuroda-Sowa, Y. Suenaga, M. Munakata, *Inorg. Chim. Acta* **2004**, *357*, 3456–3472.
[50] I. J. Bruno, J. C. Cole, P. R. Edgington, M. Kessler, C. F. Macrae, P. McCabe, J. Pearson, R. Taylor, *Acta Crystallogr. Sect. A* **2002**, *58*, 389–397.
[51] C. R. Woods, M. Benaglia, S. Toyota, K. Hardcastle, J. S. Siegel, *Angew. Chem.* **2001**, *113*, 771–773; *Angew. Chem. Int. Ed.* **2001**, *40*, 749–751; .
[52] M. Schmittel, V. Kalsani, R. S. K. Kishore, H. Colfen, J. W. Bats, *J. Am. Chem. Soc.* **2005**, *127*, 11544–11545.
[53] N. Camire, U. T. Mueller-Westerhoff, W. E. Geiger, *J. Organomet. Chem.* **2001**, *637*, 823–826.
[54] R. J. LeSuer, W. E. Geiger, *Angew. Chem.* **2000**, *112*, 254–256; *Angew. Chem. Int. Ed.* **2000**, *39*, 248–250; .
[55] R. J. LeSuer, C. Buttolph, W. E. Geiger, *Anal. Chem.* **2004**, *76*, 6395–6401.
[56] A. J. Bard, L. R. Faulkner, *Electrochemical Methods: Fundamentals and Applications*, Wiley, **2001**.
[57] J.-P. Collin, P. Laine, J.-P. Launay, J.-P. Sauvage, A. Sour, *J. Chem. Soc. Chem. Commun.* **1993**, 434–435.
[58] A. A. Vlcek, *Coord. Chem. Rev.* **1982**, *43*, 39–62.

Published online: October 10, 2007

